Analytical Magnetapheresis of Ferritin-Labeled Lymphocytes

ARTICLE *in* ANALYTICAL CHEMISTRY · NOVEMBER 1995

Impact Factor: 5.64 · DOI: 10.1021/ac00116a014 · Source: PubMed

5 AUTHORS, INCLUDING:

Ralph Green
University of California, Davis
213 PUBLICATIONS **5,742** CITATIONS
SEE PROFILE

Jeffrey J Chalmers
The Ohio State University
178 PUBLICATIONS **3,929** CITATIONS
SEE PROFILE

Anal. Chem. **1995**, *67*, 3702–3712

Analytical Magnetapheresis of Ferritin-Labeled Lymphocytes

Maciej Zborowski,*,† Chwan Bor Fuh,† Ralph Green,‡ Liping Sun,§ and Jeffrey J. Chalmers§

Departments of Biomedical Engineering, Clinical Pathology, and Cell Biology, The Cleveland Clinic Foundation, 9500 Euclid Avenue, Cleveland, Ohio 44195, and Department of Chemical Engineering, The Ohio State University, 140 West 19th Avenue, Columbus, Ohio 43210-1180

Analytical magnetapheresis is a technique for analyzing magnetic particles in suspension. The magnetically susceptible particles form a deposition pattern from the suspending medium under carefully controlled flow and magnetic field conditions. This technique was used to determine the effective magnetic volumetric susceptibility, $\Delta\chi$, of human lymphocytes labeled with an iron-rich protein, ferritin. Dynabeads M450, monodisperse polymeric beads doped with magnetite, of a diameter 4.5 μm, close to that of human lymphocytes, were used as a reference. The experiment showed an almost complete deposition of ferritin-labeled lymphocytes at an average flow velocity of 0.28 mm/s, a representative magnetic field of 1.67 T, and a magnetic field gradient of 2.57 T/mm. The calculated $\Delta\chi$ was $(2.92 \pm 0.24) \times 10^{-6}$[SI] (ferritin-labeled lymphocytes), and the corresponding number of ferritin molecules per lymphocyte was $(1.75 \pm 0.44) \times 10^7$. In comparison, an almost complete deposition of the Dynabeads was observed at a much higher average flow velocity, 15 mm/s, a much lower field, 0.164 T, and a much lower field gradient, 0.025 T/mm. These results corresponded to a much higher $\Delta\chi = 0.245$[SI] (Dynabeads M450). These results offer important guidelines in evaluating the use of ferritin as a soluble magnetic cell label.

Magnetic separation has played an important role in the manufacturing and mining industries since the nineteenth century.[1] Only recently has it been introduced to the life sciences, where it has been growing in popularity in the past decade, in particular as a technique for cell separation.[2-6] Compared to other more conventional methods of cell separation, magnetic separation is relatively simple and fast. The static magnetic field does not interfere with the movement of ions and charged solutes in aqueous solutions (at low flow rates) as does the electric field. Furthermore, the large differences between magnetic permeabilities of the magnetic and nonmagnetic materials can be exploited in developing highly selective separation methods. This high selectivity can be achieved with other separation methods only through extensive and costly instrumentation development.

Industrial magnetic separators are typically challenged by ferromagnetic particles. Almost all biological material, however, such as proteins, DNA, and cells, are either diamagnetic or slightly paramagnetic and therefore require a magnetic support for separation.[7] Notable exceptions are erythrocytes and magnetotactic bacteria because of their high iron content.[7-9] Diamagnetic substances are characterized by a negative magnetic susceptibility, χ, whereas paramagnetic substances have a positive magnetic susceptibility. The magnetic support is provided either by particulate suspension of large polymeric particles doped with magnetite or by solutions or colloidal suspension of paramagnetic compounds.

The application of large magnetic particles as a magnetic support evolved from particle-based immunoassays and tests.[3,10,11] Polymeric particles or beads are rendered magnetically susceptible by doping the polymer with magnetite. The magnetic susceptibility of such particles, typically of the order of $\chi_p = 10^{-1}$[SI], is several orders of magnitude higher than the net magnetic susceptibility of deoxygenated erythrocytes in aqueous medium, 5.17×10^{-6}.[7] (The SI unit system and the volumetric magnetic susceptibility, χ, are used throughout this study unless otherwise indicated. If χ' is in em cgs units, then χ[SI] $= 4\pi\chi'$[em cgs].) The magnetic susceptibility of the aqueous medium (water) is $\chi_{aq} = -9.05 \times 10^{-6}$ (diamagnetic).[7,13] The diameter of the magnetic beads is of the order of 1 μm, and the beads have functionalized surfaces allowing for conjugation with antibodies. The combination of a large surface area and the magnetic susceptibility of the dispersed solid phase dramatically decreases the assay time and simplifies the separation steps.[14] These large magnetic particles are rapidly displaced from a solution, even by relatively weak magnetic fields and low gradients, typically 0.1 T and 10 T/m, respectively.

* Address correspondence to this author. Telephone: (216) 445-9330. FAX: (216) 444-9198. E-mail: zborow@bme.ri.ccf.org.

† Department of Biomedical Engineering, The Cleveland Clinic Foundation.

‡ Departments of Clinical Pathology and Cell Biology, The Cleveland Clinic Foundation.

§ Department of Chemical Engineering, The Ohio State University.

(1) Mitchell, R.; Bitton, G.; Oberteuffer, J. A. *Sep. Purif. Methods* **1975**, *4*, 267–303.

(2) Hirschbein, B. L.; Brown, D. W.; Whitesides, G. M. *CHEMTECH* **1982**, March, 172–179.

(3) Funderud, S.; Nustad, K.; Lea, T.; Vartdal, F.; Guadernack, G.; Stensted, P.; Ugelstad, L. In *Lymphocytes: A Practical Approach*; Klaus G. G. B., Ed.; Oxford University Press: New York, 1987; pp 55–61.

(4) Lau, H. P.; Charlton, R. R.; Yang, E. K.; Miller, W. K. *Targeted Diagn. Ther.* **1989**, *2*, 201–216.

(5) Hancock, J. P.; Kemshead, J. T. *J. Immunol. Methods* **1993**, *164*, 51–60.

(6) Battye, F. L.; Shortman, K. *Curr. Opin. Immunol.* **1991**, *3*, 238–241.

(7) Graham, M. D. *J. Phys., Colloq.* **1984**, 45 (Suppl. au no. 1), C1:779–C1:784.

(8) Okazaki, M.; Maeda, N.; Shiga, T. *Experientia* **1986**, *42*, 842–843.

(9) Meldrum, F. C.; Mann, S.; Heywood, B. R.; Frankel, R. B.; Bazylinski, D. A. *Proc. R. Soc. London Ser. B* **1993**, *251*, 231–236.

(10) Bangs, L. B. *J. Intern. Fed. Clin. Chem.* **1991**, *2*, 188–193.

(11) Vaccaro, D. E. *Amer. Biotechnol. Lab.* **1990**, *8*, 30–35.

(12) Gee, A. P.; Mansour, V.; Weiler, M. *J. Immunogen.* **1989**, *16*, 103–115.

(13) *CRC Handbook of Chemistry and Physics*, 67th ed.; Weast, R. C., Ed.; CRC Press: Boca Raton, FL, 1986; p E-123.

(14) *Current Protocols in Immunology*; Coligan, J. E., Kruisbeek, A. M., Margulies, D. H., Shevach, E. M., Strober, W., Eds.; John Wiley and Sons: New York, 1992; pp 7.4.1–7.4.6.

0003-2700/95/0367-3702$9.00/0

The successful application of magnetic particles to immunoassays led to the evaluation of their ability to tag cells. At present, there are at least two types of particle-based immunomagnetic cell separation systems commercially available that are used in laboratory and clinical applications, Dynal MPC (Dynal, Great Neck, NY), and MaxSep magnetic cell separator (Baxter Co., Deerfield, IL). Both systems are typically used in combination with monodisperse polystyrene beads, 4.5 μm in diameter, doped with magnetite at 23% (w/v) (Dynabeads M450, Dynal A.S., Oslo, Norway). With their increasing use for cell tagging, it becomes apparent that the size of the magnetic beads, comparable to that of the cell, is an important limitation in the magnetic separation efficiency.[5] A number of studies have been reported recently in which smaller, colloidal magnetic cell labels were investigated to determine the efficiency of cell tagging.[4,15,16] A magnetic separation system based on a colloidal 50 nm diameter magnetic microbead became commercially available recently (MiniMACS, Miltenyi Biotec Inc., Sunnyvale, CA).

The rapid integration of magnetic separation techniques and new magnetic labels in biotechnology requires parallel development of analytical methods to measure and optimize the magnetic separation process. The limitation of the currently used magnetic separators is that they do not allow direct observation of the magnetic fraction. Information about the performance of such separators is always inferred indirectly from the difference in the cell population composition before and after the magnetic separation. We developed a system in which the magnetically separated cells are directly accessible to cytological and cytochemical examination on the microscopic slide. Such a system offers higher sensitivity in detecting the magnetic cell separation than the current systems. Conceptually, this system evolved from ferrography, an analytical method based on the magnetic deposition of particles in a free-flowing, open stream.[17–20] We propose the term "analytical magnetapheresis" (from Greek *apheresis*, to take off or isolate) to describe the process of magnetic separation for analytical purposes.[21–23]

The magnetic deposition system comprised intersecting fluid flow path and the magnetic interpolar gap of a permanent magnet (see Figure 1). The magnetic field of the interpolar gap was characterized by the saturation field deep inside the interpolar gap, B_0, and the interpolar gap width, $2a$. The fluid flow was contained inside a parallelpiped channel of known width, w, and height, h. A homogeneous population of cells (human lymphocytes) was magnetically labeled using a high iron content protein, cationized ferritin. Ferritin is a naturally occurring, soluble iron storage protein in mammals.[24] The cell type and the ionic character of the magnetic label binding ensured uniform magnetization of all cells in the sample. The suspensions of magnetically

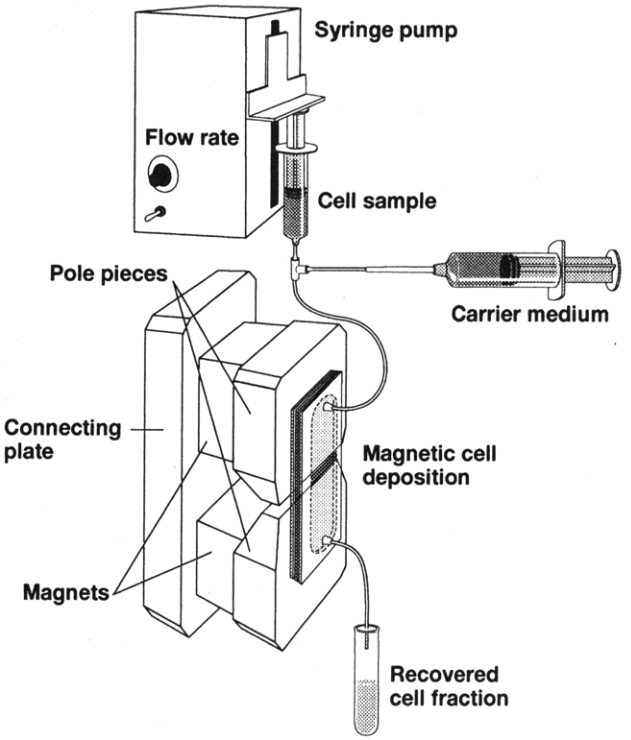

Figure 1. Principal components of analytical magnetapheresis. Before magnetic separation, the entire fluid path is filled with carrier medium. The cell sample is held in a syringe. At a controlled rate, using a syringe pump, cells are pumped into a thin parallelpiped channel placed over the magnet. The deposition of the magnetic material forms at the interpolar gap of the magnet. The magnetically trapped cells adhere to the bottom wall of the channel, after which the cells are air-fixed, stained, and mounted on slides, allowing for microscopic analysis and storage. The cells escaping the magnetic entrapment are collected in a tube past the magnet and counted.

labeled cells were pumped through the channel at various volumetric flow rates, Q. For each value of Q, the cells were counted before and after the magnetic deposition. The number of cells recovered past the magnet after the deposition, relative to the number of cells before the deposition, was defined as the fractional cell (or particle) recovery, ϵ. As a result, the rate of change of ϵ with the variation of Q was characteristic of the average net magnetic susceptibility of the cell, $\Delta\chi$. Monodisperse magnetic microspheres, Dynabeads M450, of well-characterized dimension and the magnetic susceptibility, were used as a control.[12]

The objectives of this study were to show that the magnetic field used in magnetapheresis may be mapped to a very high degree of accuracy, that such magnetic field is amenable to a highly accurate theoretical description allowing computations of the magnetic force field in the vicinity of the interpolar gap, and that the interposition of a well-defined laminar flow on the magnetic field leads to a highly controlled magnetic deposition system. We also show that the magnetically deposited cell fraction is amenable to routine cytological examination.

1. THEORY

1.1. Description of the Model. Due to high viscous forces acting on the micrometer-size cells (or particles) in the aqueous

(15) Miltenyi, S.; Müller, W.; Weichel, W.; Radbruch, A. *Cytometry* **1990**, *11*, 231–238.
(16) Yau, J. C.; Reading, C. L.; Thomas, M. W.; Davaraj, B. M.; Tindle, S. E.; Jagannath, S.; Dicke, K. A. *Exp. Hematol.* **1990**, *18*, 219–222.
(17) Seifert, W. W.; Westcott, V. C. *Wear* **1972**, *21*, 27–42.
(18) Evans, C. H.; Tew, W. P. *Science* **1981**, *213*, 653–654.
(19) Nair, K. *Basic Fluid Power Res. J.* **1980**, *13*, 281–294.
(20) Russell, A. P.; Westcott, V. C.; Demaria, A.; Johns, M. *Wear* **1983**, *90*, 159–165.
(21) Zborowski, M.; Malchesky, P. S.; Jan, T.-F.; Hall, G. S. *J. Gen. Microbiol.* **1992**, *138*, 63–68.
(22) Zborowski, M.; Tada, Y.; Malchesky, P. S.; Hall, G. S. *Appl. Environ. Microbiol.* **1993**, *59*, 1187–1193.
(23) Zborowski, M.; Tada, Y.; Malchesky, P. S.; Hall, G. S. *Colloids Surf. A: Physicochem. Eng. Aspects* **1993**, *77*, 209–218.
(24) Harrison, P. M.; Andrews, S. C.; Artymiuk, P. J.; Ford, G. C.; Lawson, D. M.; Smith, J. M. A.; Treffry, A.; White, J. L. In *Iron Transport and Storage*; Ponka, P., Schulman, H. M., Woodworth, R. C., Eds.; CRC Press: Boca Raton, FL, 1990; pp 81–102.

medium, the magnetic cells moved in a quasi-static motion (no inertial effects). Therefore, the viscous drag, $\mathbf{F}_D$, equals the magnetic force, $\mathbf{F}_m$, and the cell motion was described by the equation

$$\mathbf{F}_D = \mathbf{F}_m \tag{1}$$

The magnetic force, $\mathbf{F}_m$, acting on a cell labeled with N_{fer} identical ferritin molecules is a sum of the magnetic forces acting on each ferritin molecule, $\mathbf{F}_{fer}$:[25]

$$\mathbf{F}_m = \sum_{fer}^{N_{fer}} \mathbf{F}_{fer} \tag{2}$$

The magnetic force acting on the ferritin molecule, $\mathbf{F}_{fer}$, is the force of an external, nonuniform magnetic field, $\mathbf{B}$, acting on a magnetic dipole, μ. The magnetic dipole moment of ferritin, $\boldsymbol{\mu}_{fer}$, is induced by the external magnetic field of strength $\mathbf{H}$, and $\boldsymbol{\mu}_{fer} \propto \mathbf{H}$ (paramagnetic ferritin). In a diamagnetic medium, such as water, $\mathbf{B} = \mu_0\mathbf{H}$. The magnetic moment, magnetostatic potential energy, U, and magnetic force, $\mathbf{F}_{fer}$, acting on the ferritin molecule are expressed by the following formulae:[25]

$$\boldsymbol{\mu}_{fer} = V_{fer}\Delta\chi_{fer}\frac{\mathbf{B}}{\mu_0}, \quad U = -{}^1/_2\,\boldsymbol{\mu}_{fer}\cdot\mathbf{B} \tag{3a}$$

$$\mathbf{F}_{fer} = -\nabla U = {}^1/_2\,\frac{V_{fer}\Delta\chi_{fer}}{\mu_0}\nabla B^2 \tag{3b}$$

where V_{fer} is ferritin volume, $\Delta\chi_{fer} = \chi_{fer} - \chi_{aq}$ is the net ferritin magnetic cell susceptibility in the aqueous solution, and μ_0 is the magnetic permeability of vacuum. The cell size is small with respect to spatial variations of $\boldsymbol{B}$, and therefore the same field and gradient are acting on each ferritin molecule on the cell. Substitution of eq 3b into eq 2 yields

$$\mathbf{F}_m = N_{fer}\mathbf{F}_{fer} = {}^1/_2 N_{fer}\frac{V_{fer}\Delta\chi_{fer}}{\mu_0}\nabla B^2 \tag{3c}$$

The magnetic force acting on the cell also can be expressed by an effective cell magnetic susceptibility, $\Delta\chi$. The term "effective" here means relative to the medium (water) and averaged over the cell volume. The cell motion in the external magnetic field stems from its effective magnetic susceptibility, $\Delta\chi$, and the resulting magnetic force $\mathbf{F}_m$:

$$\mathbf{F}_m = {}^1/_2\,\frac{\Delta\chi V}{\mu_0}\nabla B^2 \tag{4}$$

where V is cell volume. Native lymphocytes have a magnetic susceptibility equal to that of water, and therefore their effective susceptibility, $\Delta\chi = 0$. Since the effective magnetic cell susceptibility is the result of binding of the ferritin molecules, it follows that the right-hand sides of eqs 3c and 4 are equal, from which one obtains

$$N_{fer}\Delta\chi_{fer}V_{fer} = \Delta\chi V$$

$$N_{fer} = \frac{\Delta\chi}{\Delta\chi_{fer}}\frac{V}{V_{fer}} = \frac{\Delta\chi}{\Delta\chi_{fe4}}\left(\frac{R}{R_{fer}}\right)^3 \tag{5}$$

where R and R_{fer} are cell and ferritin radii, respectively. The ferritin molecule comprises a protein shell of a molecular weight of 450 000 and an outer radius of 6 nm. It contains an iron core of a varying number of iron atoms, depending on species and metabolic state of the organism.[24] The commercial horse spleen ferritin preparation used in this experiment contains varying numbers of iron atoms in one ferritin molecule, from 1000 to up to 4000, with an average of 2000. This corresponds to 20% (w/w) iron content, ferritin specific gravity of 2.37 g/cm^3, and molecular weight of 560 000. The reported specific magnetic susceptibility of horse spleen ferritin at room temperature is 7.5×10^{-6}[em cgs] (no information about iron load was provided).[26] The reported molar magnetic susceptibility of the ferritin iron core is 5900×10^{-6}[em cgs] at 2000 iron atoms/ferritin molecule, corresponding to a lower value of the ferritin specific susceptibility of 2.95×10^{-6}[em cgs].[33] The corresponding value of the volumetric magnetic susceptibility in SI units, used in the subsequent calculations, is $\chi_{fer} = 4\pi(2.37)(2.95 \times 10^{-6}) = 87.9 \times 10^{-6}$. Thus, the net volumetric susceptibility of ferritin molecule in aqueous solution is $\Delta\chi_{fer} = \chi_{fer} - \chi_{aq} = 87.9 \times 10^{-6} - (-9.05 \times 10^{-6}) = 96.9 \times 10^{-6}$. In calculating N_{fer}, we used the reported average lymphocyte radius of 5 μm,[27] which was somewhat higher than the value measured in our laboratory, 4.2 ± 0.4 μm (data not shown). The error of N_{fer} relative to the presence of cells other than lymphocytes (mostly monocytes) in the lymphocyte preparation, which also bind ferritin, was accounted for by assuming the same dispersion of cell radii around the mean as observed in our laboratory, 0.4 μm (data not shown).

The source of the magnetic field is the interpolar gap of a half-width equal to a, and the saturation field deep inside the gap equal to B_0. Such a gap can be approximated by an infinite slot in a complex z-plane. The magnetic field can be described using a scalar potential P.[28] The field lines and the equipotential lines for the infinite slot were obtained using the complex potential function P of a single line current in a complex w-plane:

$$P = \Phi + j\Theta = -\frac{j}{\pi}(\Phi_2 - \Phi')\ln w + \Phi' \tag{6}$$

where Φ_2 and Φ' are constants. The constant field lines, Φ = const, and the constant potential lines, Θ = const, in the w-plane were transformed back to the complex z-plane using the conformal mapping function for an infinite slot:[28]

$$z = a + 2j\frac{a}{\pi}[\sqrt{1 - w^2} + \ln w - \ln(1 + \sqrt{1 - w^2})] \tag{7}$$

The maps of the magnetic field around the interpolar gap in the

(25) Becker, R. *Electromagnetic Fields and Interactions*; Dover Publications, Inc.: New York, 1982; Chapter CIII.

(26) Blaise, A.; Chappert, J.; Girardet, J.-L. *C. R. Acad. Sci. Paris* **1965**, *261*, 2310–2313.

(27) *Hematology*; Williams, W. J., Beutler, E., Erslev, A. J., Lichtman, M. A., Eds.; McGraw-Hill Co.: New York, 1990; Chapter 100.

(28) Weber, E. *Electromagnetic Fields. Theory and Applications. Vol. I—Mapping of Fields*; John Wiley & Sons, Inc.: New York, 1960; p 344.

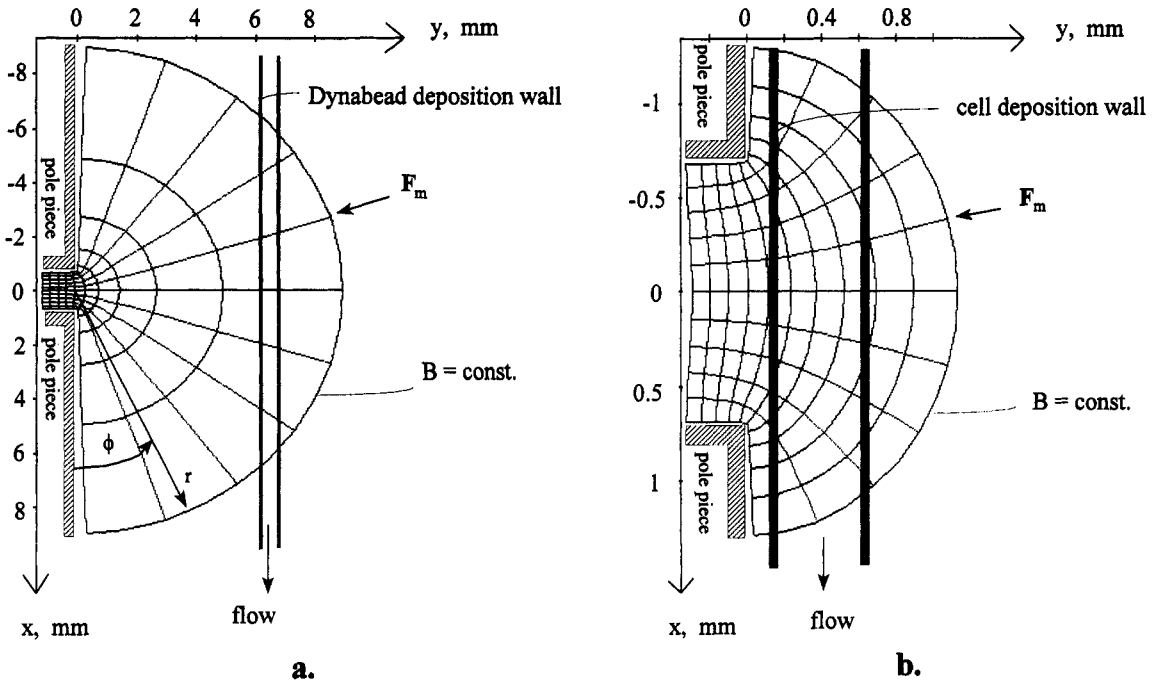

Figure 2. Magnetic field around the interpolar gap. The field lines, B, and the equipotential lines orthogonal to the field lines were generated using a solution for an infinite slot, eqs 6 and 7. The arrow shows direction of the magnetic force, F_m, acting on a small paramagnetic particle in the far field. The position of the flow channel is indicated by a pair of thick lines. The direction of the carrier medium flow is indicated by an arrow. (a) Far field, used in the Dynabead deposition experiments. The field lines are concentric semicircles, and equipotential lines are radial lines from the origin. The polar coordinates $[r,\phi]$ were used in the far-field approximation, eq 8. (b) Near field, used in the cell deposition experiments.

z-plane are shown in Figure 2 parts a (far from the interpolar gap) and b (near the interpolar gap).

The surfaces of the pole pieces near the gap may be treated as the equipotential surfaces.[28] At distances greater than a, the near-field map shown in Figure 2b was approximated by the far-field map shown in Figure 2a. For the far field, the following relationship holds:[28]

$$\mathbf{B} = \frac{2aB_0}{\pi}\frac{1}{r}\frac{\mathbf{r}}{r} \tag{8}$$

where $\mathbf{r} = [x,y]$ is the position vector of the magnitude $r = (x^2 + y^2)^{1/2}$.

The cell motion in the viscous medium was approximated by that of a rigid sphere of radius R. The cell motion was within the Stokes region, since the product of the cell velocity relative to that of medium, Δv, and cell diameter, $2R$, was less than about 0.01 cm^2/s.[29] The viscous drag force was represented by the Stokes formula:

$$\mathbf{F}_D = 6\pi R\eta\Delta v \tag{9}$$

The carrier medium velocity distribution in a parallelpiped channel of very large aspect ratio (width to height, $w/h \approx 12$)) was parabolic, thus,

$$v_x(y) = -\frac{4v_{max}}{h^2}(y - y_1)(y - y_2) \tag{10a}$$

$$v_{max} = {}^3/_2\frac{Q}{wh} \tag{10b}$$

where v_{max} is the maximum flow velocity, $h = y_2 - y_1$ is the height of the rectangular channel, w is the width of the channel, and Q is the volumetric flow rate of the carrier medium.

1.2. Trajectories of the Magnetically Labeled Cells in the Magnetic Field and the Fractional Cell Recovery, ϵ. The fractional cell recovery, ϵ, was defined as the ratio of cell concentration in the eluate, c_{out}, to that in the feed, c_{in}:

$$\epsilon = c_{out}/c_{in} \tag{11}$$

The value of ϵ was computed numerically by simulating particle trajectories in the magnetic and flow fields. The trajectories were simulated for different initial positions of the particle (cell) upstream, far away from the interpolar gap. The initial position of the cell with respect to the deposition wall was defined by the parameter λ, $0 < \lambda < 1$, so that $y_0 = y_1 + \lambda h$ is the initial y-coordinate of the cell, where y_1 is the position of the deposition wall, and h is the channel height (see Figure 2). The initial position of the cell the most distant from the deposition wall, trapped by the magnetic field, was denoted λ_0. For a parabolic flow velocity distribution, eq 10, one obtains

$$\epsilon = c_{out}/c_{in} = 1 - \frac{\int_{y_1}^{y_1+\lambda_0 h} c_{in}v_x(y)\,dy}{\int_{y_1}^{y_2} c_{in}v_x(y)\,dy} = 1 - (3\lambda_0^2 - 2\lambda_0^3) \tag{12}$$

where $y_2 = y_1 + h$.

Equation 1, with the substitutions of eqs 4, 8, 9, and 10, was solved in the $x'y'$-plane, using dimensionless variables x', y', t', and

(29) Bird, B. R.; Stewart, W. E.; Lightfoot, E. N. *Transport Phenomena*; John Wiley and Sons: New York, 1960; Chapter 2.6.

B', defined as follows:

$$x' = x/a, \quad y' = y/a, \quad t' = (v_{max}/a)t,$$
$$B' = B/B_0 = (2/\pi)(1/r') \tag{13}$$

The relationship between the primed and nonprimed time and spatial derivatives has the following form:

$$\begin{cases} x' = \dfrac{dx'}{dt'} = \dfrac{1}{v_{max}}\dfrac{dx}{dt} = \dfrac{1}{v_{max}}x \\ y' = \dfrac{dy'}{dt'} = \dfrac{1}{v_{max}}\dfrac{dy}{dt} = \dfrac{1}{v_{max}}y \end{cases} \tag{14a}$$

$$\begin{cases} \dfrac{\partial B'^2}{\partial x'} = \dfrac{a}{B_0^2}\dfrac{\partial B^2}{\partial x} = -\dfrac{8}{\pi^2}\dfrac{x'}{r'^4} \\ \dfrac{\partial B'^2}{\partial y'} = \dfrac{a}{B_0^2}\dfrac{\partial B^2}{\partial y} = -\dfrac{8}{\pi^2}\dfrac{y'}{r'^4} \end{cases}$$

where $r' = (x'^2 + y'^2)^{1/2}$. The dimensional parameters of the system were conveniently grouped in the dimensionless number ζ, defined as follows:

$$\zeta = {}^1/_9 \frac{R^2}{\eta v_{max}} \frac{\Delta\chi}{\mu_0} \frac{B_0^2}{a} \tag{14b}$$

The equations describing the cell motion, and the initial conditions take the following form:

$$\begin{cases} x' = -\zeta\dfrac{\partial B'^2}{\partial x'} - 4\dfrac{a}{h}(y' - y'_1)(y' - y'_2) \\ y' = -\zeta\dfrac{\partial B'^2}{\partial y'} \end{cases} \tag{15}$$

$$\begin{cases} x'(0) = \dfrac{x_0}{a} \\ y'(0) = \dfrac{y_0}{a} = y'_1 + \lambda\dfrac{h}{a}, \quad 0 < \lambda < 1 \end{cases}$$

The solution of eqs 15 also determined cell trajectories and their end points in terms of parameters λ and ζ. There were two trajectory end points significant for the present analysis: either on the deposition wall, corresponding to the cell capture, or in infinity, resulting in cell recovery. By running a series of simulations for the increasing values of λ, at constant ζ, an escape value of λ_0 was determined for which the trajectory end point jumped from the deposition wall to infinity. The value of λ_0 was used subsequently to calculate ϵ, eq 12. The procedure was then repeated for a number of values of parameter ζ, resulting in a range of values of ϵ, from that approaching 0 to that approaching 1. The whole process led to the determination of a theoretical dependence of ϵ on ζ, which was conveniently presented as a plot $\epsilon = \epsilon(\zeta)$. In the remainder of the text, such plots are referred to as "calibration plots". In experiments with the ferritin-labeled lymphocytes, the calibration plot was obtained using a trial value of $\Delta\chi = 10^{-6}$. The numerical values of other parameters used in the calculations are shown in Table 1. Considering that ζ is inversely proportional to v_{max}, eq 14b, and therefore to Q, eq 10b, the relationship between ϵ and ζ could also be determined experimentally. Fitting the theoretical curve, $\epsilon = \epsilon(\zeta)$, to the experimental data was done by correcting the trial value of $\Delta\chi$ to a value for which the theoretical curve best approximates the experimental data (see below). The trial value of $\Delta\chi$ for the Dynabead M450 was set equal to the value provided by the manufacturer, $\Delta\chi = 0.245$, and no further fitting was done. Examples of cell trajectories for different values of λ_0 are shown in Figure 3.

1.3. Fitting the Calibration Curve $\epsilon = \epsilon(\zeta)$ to the Experimental Data. Two different calibration curves, $\epsilon = \epsilon(\zeta)$, one for Dynabead M450 and one for the cell, were calculated. The relative positions of the flow channel and the interpolar gap used in the calculations are shown in Figures 2, parts a and b, correspondingly. The value of λ_0, describing the most distant cell captured in the magnetic field, was evaluated with an accuracy of ± 0.01. The numerical calculations and trajectory plotting were performed using MapleV release 2 software package (MathSoft Inc., Cambridge, MA), on an IBM-compatible PC. The computer program is available from the authors on request. The sample results are illustrated in Figure 3.

Comparison between the calculated and the experimentally measured values of ϵ was made possible by expressing ζ as a function of Q. Substituting the expression for v_{max}, eq 10b, into the definition of ζ, eq 14b, yields

$$\zeta = \frac{2}{27}\frac{whR^2}{\eta}\frac{\Delta\chi}{\mu_0}\frac{B_0^2}{a}\frac{1}{Q} = \zeta_Q\frac{1}{Q} \tag{16}$$

For Dynabead M450, the computed relationship $\epsilon = \epsilon(\zeta)$ was linear for the entire range of ϵ, $0 < \epsilon < 1$. The proportionality constant, ζ_Q, eq 16, was calculated using the numerical value of $\Delta\chi_D \approx \chi_D = 0.245$, and was $\zeta_Q = 211$ mL/min. Numerical values of other constants used in the calculations are shown in Table 1. The experimental values of ϵ vs Q for Dynabeads were plotted directly onto the Dynabead calibration curve $\epsilon = \epsilon(\zeta)$ using the relationship $\zeta = \zeta_Q(1/Q)$.

For the cell, the computed relationship $\epsilon = \epsilon(\zeta)$ was almost linear in the range $0 < \epsilon \leq 0.6$. Therefore, it was approximated by the following equation:

$$\epsilon = \epsilon(\zeta) = m\zeta + b \tag{17}$$

where m is the slope and b is the intersect determined by the regression analysis for a set of points $[\zeta_i, \epsilon_i(\zeta_i)]$, $i = 1, \ldots, 10$, selected from the curve $\epsilon = \epsilon(\zeta)$, $0 < \epsilon \leq 0.6$. These values were $m = -5.41 \pm 0.25$, $b = 0.695 \pm 0.027$, and $r^2 = 0.987$. The proportionality constant, ζ_Q, calculated using the trial value of $\Delta\chi = 10^{-6}$, was equal to 2.25×10^{-3} mL/min. Other constants are shown in Table 1.

The experimental value of the cell magnetic susceptibility, $\Delta\chi$, was determined as follows. By substituting the expression for ζ, eq 16, into the expression for ϵ, eq 17, one obtains

$$\epsilon = m\zeta + b = m\zeta_Q\frac{1}{Q} + b \qquad \text{theory} \tag{18}$$

$$\epsilon_E = m_E\zeta_E + b_E = m_E\zeta_{QE}\frac{1}{Q_E} + b_E$$
$$= m'\frac{1}{Q_E} + b_E \qquad \text{experiment}$$

Table 1. Material and Geometric Parameters of the Analytical Magnetapheresis

parameter	notation	numerical value	SI units
	A. Magnetic Separation System		
interpolar gap width	a	0.7	mm
saturation magnetic field	B_0	2.433 ± 0.037	Tesla (tesla) = N A^{-1} m^{-1}
magnetic permeability of vacuum	μ_0	$4\pi \times 10^{-7}$	T·m/A
water viscosity	η	10^{-3}	kg m^{-1} s^{-1}
flow channel height	$h = y_2 - y_1$	0.5	mm
flow channel width	w	6	mm
	B. Dynabead Calibration Plot Parameters		
magnetic susceptibility	$\Delta\chi_D \approx \chi_D$	0.245	1
density	ϱ	1.5×10^3	kg/m^3
radius	R_D	2.25	μm = 10^{-6} m
volumetric flow rate of the medium	Q	2.7–20	mL/min
average flow velocity	$v_{av} = 10^3/60\ Q/w\ h$	15–110	mm/s
initial conditions	$x_0 = -10a$	$y_1 = 6.1$	mm
	$y_1 < y_0 < y_2$	$y_2 = 6.6$	
	C. Cell Calibration Plot Parameters		
effective magnetic susceptibility (trial value)	$\Delta\chi$	10^{-6}	1
density	ϱ	10^3	kg/m^3
radius	R	5	μm = 10^{-6} m
volumetric flow rate of the medium	Q	0.05–0.24	mL/min
average flow velocity	$v_{av} = 10^3/60\ Q/w\ h$	0.28–1.33	mm/s
initial conditions	$x_0 = -4a$	$y_1 = 0.15$	mm
	$y_1 < y_0 < y_2$	$y_2 = 0.65$	

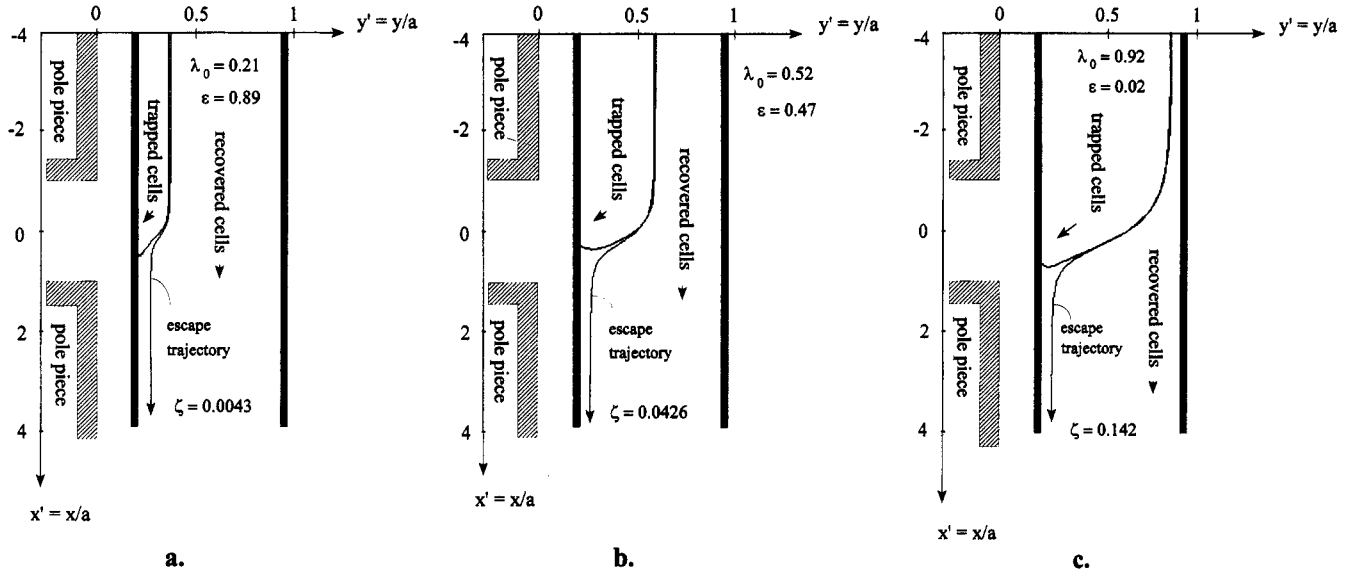

Figure 3. Examples of cell trajectories as a function of the dimensionless number ζ, defined in eq 14b. The trapped cell trajectory end points are on the deposition wall. The escape trajectory end points are in infinity. Parameter λ_0 describes the initial position at entry of the most distant cell from the deposition wall that becomes trapped. The flow of the carrier medium is from top to bottom. The panels a, b, and c are in the order of decreasing fractional cell recovery, ϵ, corresponding to increasing ζ. These panels are examples of a series of plots used to establish the Dynabead and cell calibration curves $\epsilon = \epsilon(\zeta)$, as described in the text.

The symbols with subscript E relate to the experimental quantities. The symbols without subscripts relate to the theoretical quantities. The slope, $m' = m_E\ \zeta_{QE}$, and the intersect, b_E, were determined experimentally by the regression analysis on the data points $[1/Q_E,\epsilon_E]$.

The theoretical regression line fits the experimental points if the following conditions hold true:

$$m_E = m \qquad \zeta_E = \zeta + (b - b_E)/m \tag{19}$$

From eqs 16, 18, and 19,

$$\frac{\Delta\chi_E}{\Delta\chi} = \frac{\zeta_{QE}}{\zeta_Q} \qquad \zeta_{QE} = \frac{m'}{m_E} = \frac{m'}{m} \tag{20}$$

from which one arrives at the following relationship between the experimental (corrected), $\Delta\chi_E$, and the trial, $\Delta\chi$, values of the magnetic susceptibility:

$$\Delta\chi_E = \frac{m'}{m}\frac{\Delta\chi}{\zeta_Q} \tag{21}$$

where m' is determined from experiment (see eq 18), and m, $\Delta\chi$, and ζ_Q are known from theory. Equations 19 allow one to plot the experimental data $[\zeta_E,\epsilon_E]$ against the theoretical curve $\epsilon = \epsilon(\zeta)$.

1.4. Error Analysis. All experimental measurements were done at least in duplicate. Dynabead and ferritin-labeled lymphocyte counts were repeated eight times for each value of the volumetric flow rate Q. The results are presented as averages ± standard deviation. The correlation between variables were analyzed using regression analysis at the confidence level $p = 0.05$. The regression plots show average values of the dependent variable and standard deviations. For fewer than eight measurements per independent variable, all the data points are shown. The error of the compound variable was calculated using the compound error of a function.[30] The standard deviation of the regression slope and the regression constant were used in calculating the error of the compound variable, where applicable.

2. EXPERIMENTAL SECTION

2.1. Magnetic Field Measurements. A magnetic field was generated with a permanent magnet assembly consisting of two pairs of neodymium–iron–boron magnets characterized by a maximum energy product of 2.23×10^5 T·A/m. The magnets were connected by soft iron pole pieces conducting the magnetic flux lines to the interpolar gap (see Figure 1). The length of the interpolar gap along the *Oz*-coordinate, 25 mm, was much larger than its width along the *Ox*-coordinate, $2a = 1.4$ mm (compare Figure 2), and therefore the magnetostatic field **B** was two-dimensional, in the *Oxy*-plane, near the center of the interpolar gap. The depth (along the *Oy*-coordinate) to width ratio of the interpolar gap, 6 mm:1.4 mm, was sufficient to assume that the interpolar gap field was equivalent to a field of an infinite slot. The magnetic field map shown in Figure 2 was obtained using the solutions for an infinite slot, eqs 6 and 7.

The magnetic field measurements were performed using a Gaussmeter and a Hall-effect probe (Model 9200 Gaussmeter and transverse probe STG920404, F. W. Bell, Orlando, FL). The probe measured magnetic flux perpendicular to a sensing area of a diameter 0.89 mm, located 0.37 mm from the end of the rectangular probe stem. Polar coordinates $[r,\phi]$ (see Figure 2a) were used to define the location of the center of the sensing area. The dimensions of the stem were length 100 mm, width 3.8 mm, and thickness 1.0 mm. One set of field measurements was performed along selected isomagnetic lines, B = const, far from the interpolar gap. In the far-field region, the isomagnetic lines form concentric semicircles centered on the origin, similar to the field lines B (see Figure 2b). The measurements were performed at three different distances from the center of the interpolar gap, $r = 5$, 10, and 20 mm, and for varying ϕ at constant r, from $\phi = 15°$ to 165°, in 15° increments. The probe was mounted on a cutout which assured the perpendicular orientation of the probe sensing area to the magnetic field lines at any given set of the polar coordinates $[r,\phi]$. A separate set of measurements was performed for varying r at constant ϕ, from $r = 0$ to 20 mm, in increments from 0.02 mm in the fast changing field region to 0.4 mm in the slow changing region. The probe was mounted on a micrometer stage (Klinger Scientific, Richmond Hill, NY).

The saturation field deep inside the gap, B_0, was calculated by analyzing the dependence of B over $1/r$. The slope of the regression line B over $1/r$, in the linear range of B vs $1/r$, determined the value of B_0 for the known value of a, see eq 8. The $B \propto 1/r$ approximation of the magnetic field was accurate for experiments with Dynabeads for which the deposition channel was placed in the far field of the slot, from $y_1 = 6.1$ mm to $y_2 = 6.6$ mm. The $B \propto 1/r$ approximation could be used down to distances of $r = (0.34)2a = 0.68 \times 0.7\text{mm} = 0.48$ mm, at which the slot flux changes character to the tooth tip flux.[28] This approximation was also used in calculating the reference cell calibration curve, $\epsilon = \epsilon(\zeta)$. The error in using expressions 8 instead of the exact solution of eq 6 and 7 was approximately 10% (data not shown) for the most distant cell from the interpolar gap, for which $y_0 = 0.65$ mm. The large errors in predicting ϵ at high flow rates due to the contribution of cells close to the slot was avoided by limiting the analysis to $\epsilon \leq 0.6$.

The characteristic values of the magnetic field, B, and gradient, $|\nabla B|$, see eqs 8, were determined at the field line corresponding to the most distant cell trajectory from the interpolar gap. In Dynabead experiments, this corresponded to the distance $r = 6.6$ mm; for experiments with the ferritin-labeled lymphocytes, this corresponded to the distance $r = 0.65$ mm.

2.2. Flow Channel. The flow channel consisted of top and bottom plates and a silicone rubber spacer. The spacer was sandwiched between the top and bottom plates. The top plate had two drilled holes to connect the tubing used as an inlet and an outlet for the channel. The bottom plate was made of a thin glass, 150 μm thick (Fisher Finest Premium Cover Glass No.1, Fisher Scientific, Pittsburgh, PA), and was used to collect the magnetic deposition. The cutout of the silicone rubber sheet (Silastic 0.02 in., Dow Corning Corp., Midland, MI) of length 40 mm and width 6 mm was used as a flow channel chamber. The spacer thickness defined the flow channel height, $h = 0.5$ mm.

The flow channel was positioned at two different distances from the magnet surface. In the experiments with ferritin-labeled lymphocytes, the distance from the inner surface of the deposition plate to the magnet was $y_1 = 0.15$ mm. In experiments with the M450 beads, this distance was $y_1 = 6.1$ mm.

The volumetric flow rates used in the lymphocyte experiments were $Q = 0.05$, 0.07, 0.10, 0.15, and 0.24 mL/min. These flow rates corresponded to the linear velocity range of 0.28–1.3 mm/s. The volumetric flow rates used for the experiments with M450 beads were $Q = 2.7$, 3.9, 5.9, 8.8, 13, and 20 mL/min, corresponding to the linear flow velocity range of 15–110 mm/s.

The flow channel was positioned such that the flow direction was parallel to gravity to avoid interference from gravitational sedimentation. After each experiment, the bottom plate was disassembled and stained with Modified Wright stain (Sigma Chemical Co., St. Louis, MO) before being mounted on microscope slides.

2.3. Lymphocytes and M450 Reference Beads. Freshly drawn blood was obtained from consenting, healthy volunteer donors according to institutional guidelines. Peripheral lymphocytes were isolated from whole blood using density gradient centrifugation (Ficoll-Hypaque, Pharmacia, Piscataway, NJ) immediately after blood donation. The residual erythrocytes were lysed by exposure for 1 min to an osmotic shock buffer (RBC Lysing Buffer, Sigma Chemical Co.). The lymphocytes were washed several times with phosphate-buffered saline (PBS, GIBCO, Grand Island, NY) and kept on ice until needed for use. The composition of the cell sample was evaluated for selected samples using an automated cell counter (Technicon Co., Tarrytown, NY), and it showed 95% lymphocytes (including both T and B subpopulations); the remaining fraction was mostly monocytes

(30) Margenau, H.; Murphy, G. M. *The Mathematics of Physics and Chemistry*; D. Van Nostrand Co.: Princeton, NJ, 1962; Chapter 13.

with a small number of neutrophils. The magnetic labeling technique, described below, was not specific to the cell surface markers; therefore, on average, the amount of the label bound per cell surface area was approximately the same for all markers. Larger cells, such as monocytes, would acquire more label and therefore contribute more to the deposition than their fractional concentration in solution. This effect of the cell size on the cell susceptibility analysis was considered small, however, due to only a small number of monocytes in the sample and the uniform size of the normal peripheral lymphocytes.[27]

The lymphocytes were incubated with cationized horse spleen ferritin (Sigma Chemical Co.) in 25 mM HEPES and 150 mM NaCl solution (pH = 7.5) at room temperature for 15 min. The cationized ferritin is supplied as a *N,N*-dimethyl-1,3-propanediamine derivative of the native horse spleen ferritin, and it exhibits a net positive charge at pH 7.5. Under these conditions, the cationized ferritin readily formed ionic bonds with the anionic sites on the cell membrane.[33] The concentration of ferritin was 0.001% (v/v). Following incubation, lymphocytes were washed with 150 mM NaCl to remove ferritin from solution. The lymphocyte counts were performed using a hemacytometer (Reichert, Buffalo, NY) before and after the magnetic deposition experiments. The sample volume was 0.5 or 1.0 mL. The initial lymphocyte concentration was 2×10^6 cells/mL; the initial M450 bead concentration was 1×10^6 beads/mL. The fractional cell recovery, ϵ, in the fraction collected past the magnet was calculated as the ratio of cell counts in the recovered cell sample to cell counts in the initial cell sample, in accordance with eq 11. The values of ϵ were plotted as a function of $1/Q$ and fitted to the reference cell calibration curve $\epsilon = \epsilon(\zeta)$ as discussed in section 1.3 above.

3. RESULTS

3.1. Magnetic Field. The magnetic field as a function of ϕ, $B = B(\phi)_r$, at three different polar distances r from the interpolar gap center, is shown in Figure 4a. As expected from the theory, there was very little variation in B as a function of ϕ in the far-field region. The following averages were obtained at different distances r from the center of the gap: $\langle B(\phi)_r \rangle = 0.316 \pm 0.014$ T at $r = 5$ mm, $\langle B(\phi)_r \rangle = 0.175 \pm 0.010$ T at $r = 10$ mm, and $\langle B(\phi)_r \rangle = 0.0894 \pm 0.0070$ T at $r = 20$ mm. The magnetic field variation with distance r at $\phi = 0$ is shown in Figure 4b. The far-field approximation, $B \propto 1/r$, starts to break down at distances of ~1 mm, where the field bends toward a plateau inside the interpolar gap. The far-field region is shown in Figure 4c using a plot of B on $1/r$, at $\phi = 0$, for $r = 1$–20 mm. Again, the departure from nonlinearity is noticeable at $r = 1$ mm. The slope of the regression line of B on $1/r$ at $\phi = 0$ was used to determine the saturation magnetic field, B_0. The extrapolated value of the saturation magnetic field $B_0 = 2.433 \pm 0.027$ T, $n = 201$. The magnetic field B and gradient $|\nabla B|$, representative of experiments with Dynabeads (at $r = 6.6$ mm), were $B = 0.1642 \pm 0.0056$ T and $|\nabla B| = 0.024\,88 \pm 0.000\,85$ T/mm. The field and gradient representative of experiments with the ferritin-labeled lymphocytes ($r = 0.65$ mm) were $B = 1.667 \pm 0.057$ T and $|\nabla B| = 2.565 \pm 0.088$ T/mm.

3.2. Dynabead M450 Fractional Recovery. The experimental fractional recovery values, ϵ_E, were plotted as a function of ζ_E, calculated from eq 18, based on the constants listed in Table 1. The experimental points $[\zeta_E, \epsilon_E]$ were plotted directly onto the calibration curve $\epsilon = \epsilon(\zeta)$ predicted from theory, as described in section 1.3 (see Figure 5a). The theoretically predicted calibration curve was inside the 95% confidence intervals of the mean ϵ_E for

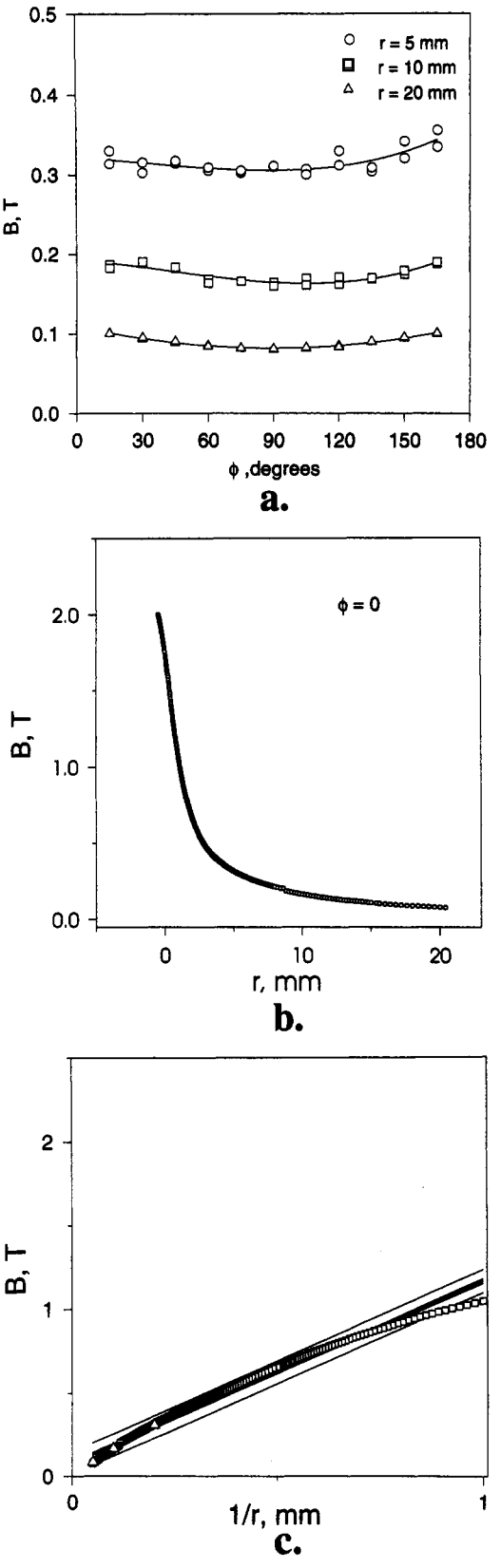

Figure 4. (a) Magnetic field, B, around the interpolar gap as a function of position in polar coordinates $[r,\phi]$ defined in Figure 2a. The field was measured along the field lines, B (see Figure 2a). Variations of the field with ϕ at constant r illustrate deviations of the experimental data from the potential field model (far field). (b) Magnetic field as a function of r, at $\phi = 0$, $n = 256$. (c) Magnetic field as a function of $1/r$ at $\phi = 0$. The triple line represents linear regression of B on $1/r$, slope = 1.083 ± 0.012, constant = 0.081 ± 0.042, $r^2 = 0.984$, and $n = 201$. The single lines represent the 95% confidence interval from the regression line. Open triangles represent average values of B shown in panel a.

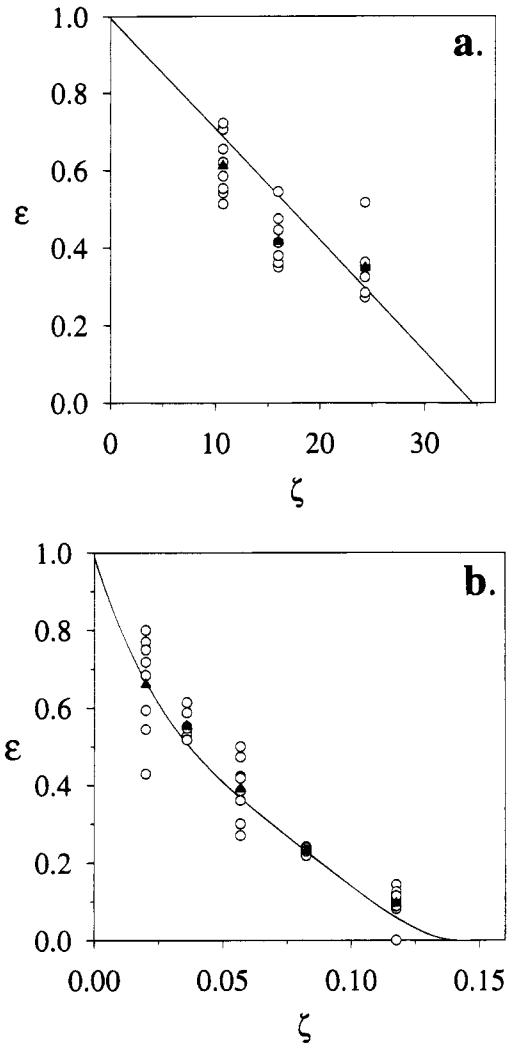

Figure 5. Calibration curve of fractional recovery, ϵ, as a function of parameter ζ, $\epsilon = \epsilon(\zeta)$. Solid lines represent theoretical prediction, open circles represent experimental observations, and solid triangles are averages for each value of ζ. (a) Dynabead M450: the theoretical values fall within the 95% confidence interval of the average experimental observations. (b) Ferritin-labeled lymphocytes: the experimental data were fitted to the theoretical calibration curve using eqs 18, see text.

all three values of ζ_E and is shown in Figure 5a, $n_E = 24$. The agreement between the predicted and measured values of the reference particle recovery, to within the experimental error, supports the validity of the results obtained for the ferritin-labeled lymphocytes.

3.3. Ferritin-Labeled Lymphocytes Fractional Recovery. The experimental points $[\zeta_E,\epsilon_E]$ were fitted onto the calibration curve $\epsilon = \epsilon(\zeta)$ predicted from theory, as described in section 1.3 (see Figure 5b). The parameters of the regression line ϵ_E on $1/Q_E$, eq 18, were the following: $m' = -(3.55 \pm 0.24) \times 10^{-2}$, $b_E = 0.773 \pm 0.043$, and $n_E = 40$. The corresponding net magnetic susceptibility of the ferritin-labeled lymphocytes was obtained from eq 21: $\Delta\chi = (2.92 \pm 0.24) \times 10^{-6}$. The corresponding average number of ferritin molecules per ferritin-labeled lymphocyte was obtained from eq 5: $N_{fer} = (1.75 \pm 0.44) \times 10^7$.

Figure 6a shows the macroscopic appearance of the magnetic deposition of M450 beads, obtained at the flow velocity of 15 mm/s. It is worth noting that this deposition was obtained when the flow channel was kept at 6.1 mm away from the magnet, as depicted in Figure 2a. The loss of beads in parts of the deposition band was an artifact of channel handling caused by the lack of bead adhesion to the channel surface.

The magnetic deposition zone for ferritin-labeled lymphocytes, after staining and mounting on the substrate slide, is shown in Figure 6c. A series of depositions is shown in order of decreasing flow velocity, from 0.83 through 0.28 mm/s. As flow velocity decreased, the density of the deposition increased. These changes corresponded to the changes in the recovered cell fraction counts, ϵ, which decreased with the decreasing flow velocity (and increasing ζ); see Figure 5b. One may also distinguish increased deposition at the edges of individual deposition bands, corresponding to the edges of the interpolar gap, (compare Figure 2b). This increase suggests that at distance a very close to the edges of the interpolar gap, the tooth tip flux dominates over the slot field flux, and the approximation $B \propto 1/r$ is no longer valid.[28] The near-field map shown in Figure 2b illustrates well the increased concentration of field lines and equipotential lines around the edge tip corresponding to the increased magnetic field, gradient, and force at the tip. However, the overall magnetic deposition appearance in Figure 6c shows the predominance of the slot effects, over tooth tip effects which supports the validity of the theoretical approach in describing the magnetic deposition process.

The microscopic appearance of cells and M450 beads in the magnetic deposition is shown in Figure 7. A concatenation of the M450 beads in the direction of the magnetic flux lines is clearly visible; it was caused by attraction between the high magnetic moments of the individual beads.

4. DISCUSSION

Analytical magnetapheresis of ferritin-labeled lymphocytes allowed close scrutiny of the magnetic separation process. The apparatus and magnetic separation were amenable to a detailed experimental and theoretical analysis. Such an analysis is rarely possible with existing magnetic separators, and relatively few attempts of such an analysis have been reported in the literature.[7,8,31-35] The measurement was done against a control provided by the reference magnetic particles, Dynabeads M450.[12] Analytical magnetapheresis allowed us to perform measurements under conditions matching possible applications of ferritin as a magnetic cell label. Low flow velocity, 0.28 mm/s, and high field intensity, 1.67 T, and high gradient, 2.57 T/mm, were required to remove ferritin-labeled lymphocytes from solution. In contrast, the M450 beads were removed almost completely at a much higher flow velocity, 15 mm/s, lower magnetic field intensity, 0.16 T, and lower gradient, 0.025 T/mm.

The low magnetic susceptibility of the ferritin-labeled cells requires that a high magnetic gradient be used to displace the cells from solution. The motion of low-susceptibility particles in the vicinity of a high-gradient magnetic field has been studied in the past using high-permeability intrusion (typically, a wire) in the magnetic field.[32-34] Use of a single wire allowed direct

(31) Hardwick, R. A.; Prisco, M. R.; Shah, D. O. *Artif. Organs* **1990**, 14, 342–347.
(32) Takayasu M.; Duske, N.; Ash, S. R.; Friedlaender, F. J. *IEEE Trans. Magn.* **1982**, *18*, 1520–1522.
(33) Odette, L. L.; McCloskey, M. A.; Young, S. H. *Biophys. J.* **1984**, *45*, 1219–1222.
(34) Takayasu, M.; Kelland, D. R. *IEEE Trans. Magn.* **1986**, *22*, 1125–1127.
(35) Liberti, P. A.; Feeley, B. P. In *Cell Separation Science and Technology*; Compala D. S., Todd, P., Eds.; ACS Symposium Series 464; American Chemical Society: Washington, DC, 1991; pp 269–289.

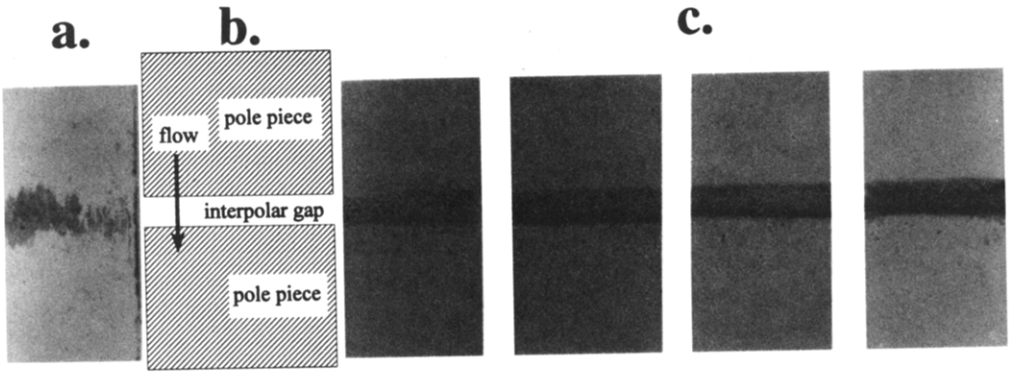

Figure 6. Macroscopic appearance of the magnetic deposition zone. The sample flow was from top to bottom. (a) M450 beads, without staining or mounting. (b) Diagram of the magnetic deposition zone, shown on the same scale as parts a and c of this figure. (c) Ferritin-labeled lymphocytes, after being stained and mounted on a microscopic slide, in the order of decreasing flow velocity, v_{av} = 0.83, 0.56, 0.39, and 0.28 mm/s, respectively. Cell deposition increased as flow velocity decreased.

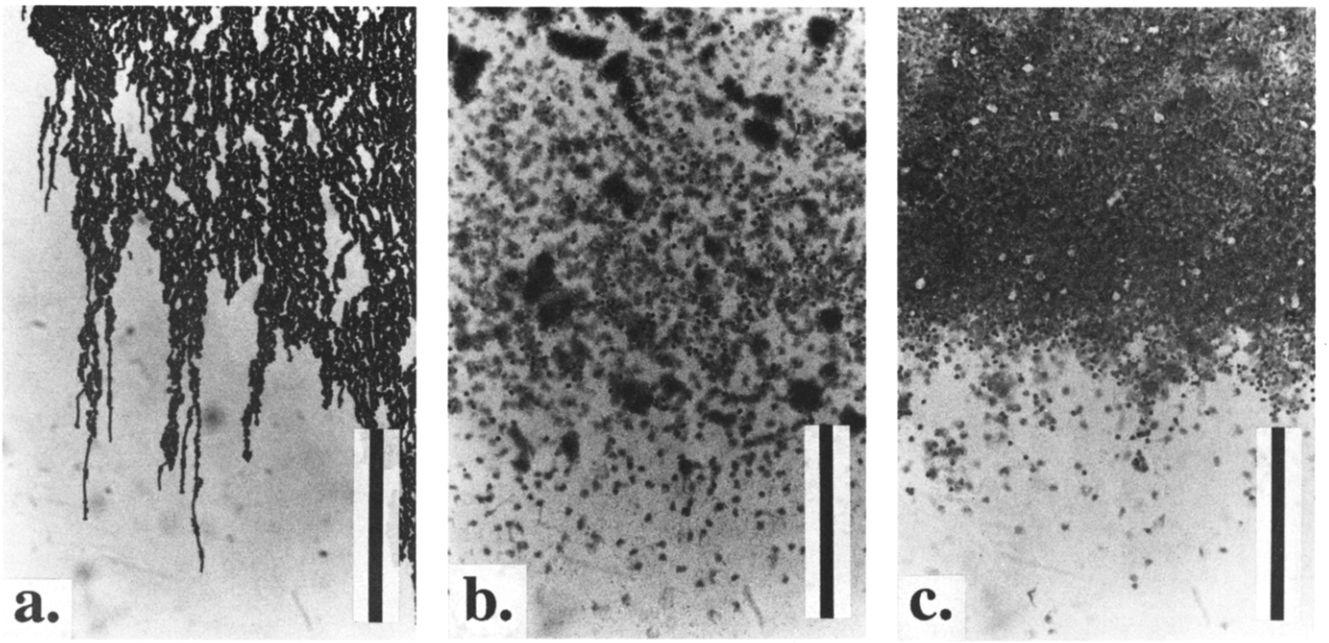

Figure 7. Microscopic appearance of the magnetic deposition shown in Figure 6. The scale bar represents 500 μm. (a) M450 Dynabeads. (b) Ferritin-labeled lymphocytes, v_{av} = 0.83 mm/s. (c) Ferritin-labeled lymphocytes, v_{av} = 0.28 mm/s. Note the comparable size of lymphocytes and M450 beads and the concatenation of M450 beads in the direction of the magnetic flux lines.

observation, on a microscopic scale, of particle deposition on the wire surface. The single high-permeability wire exposed to a homogeneous magnetic field offered a relatively simple model of the distribution of the magnetic field and forces.[36] The laminar flow of a carrier medium perpendicular to the straight, infinite wire provided a relatively simple model of the magnetic force in those studies. The formidable difficulties in extending such a model to the packed-bed, high-gradient magnetic separators and other types of magnetic separators currently in use hampered extending such an analysis to practical devices.

In this study, we used analytical magnetapheresis to compare magnetic properties of a well-characterized magnetic polymeric bead and a high iron content protein, ferritin. The use of ferritin as a magnetic cell label has been proposed before.[33,37,38] Ferritin offers several potential advantages over particulate magnetic labels and other currently evaluated colloidal magnetic labels. The structure of the protein shell of ferritin molecules provides monodisperse molecular size distribution and good solubility under physiological conditions.[24] The surface of the protein shell may be modified to form direct or indirect binding with antibodies against selected cell or tissue surface receptors. Ferritin-conjugated antibodies have been routinely used as immunological markers in transmission electron microscopy studies of cellular substructures.[39]

The studies of the magnetic properties of mammalian ferritins by Mössbauer spectroscopy and NMR spectroscopy showed that the ferrihydrite crystal has a single-domain antiferromagnetic character, accounting for the paramagnetic behavior of mammalian ferritin in the magnetic field at room temperature.[40] The chemical composition and crystalline structure of the iron compound inside the ferritin protein shell are fairly labile and may be modified to

(36) Watson, J. H. P. *J. Appl. Phys.* **1973**, *44*, 4209–4213.
(37) Russell, A. P.; Evans, C. H.; Westcott, V. C. *Anal. Biochem.* **1987**, *164*, 181–189.
(38) Zborowski, M.; Malchesky, P. S.; Savon, S. R.; Green, R.; Hall, G. S.; Nosé, Y. *Wear* **1990**, *142*, 135–149.
(39) de Petris, S.; Raff, M. C. *Eur. J. Immunol.* **1972**, *2*, 523–535.
(40) Bizzi, A.; Brooks, R. A.; Brunetti, A.; Hill, J. M.; Alger, J. R.; Miletich, R. S.; Francavilla, T. L.; Di Chiro, G. *Radiology* **1990**, *177*, 59–65.

form a single superparamagnetic magnetite crystal.[41]

Analytical magnetapheresis allowed us to calculate the magnetic susceptibility of the ferritin-labeled lymphocytes and to estimate the number of ferritin molecules per lymphocyte necessary for the magnetic cell deposition. Previous studies evaluated the feasibility of ferritin as a label for magnetic cell separation without providing information on the cell ferritin load needed to achieve separation.[33,37,38] Under the present experimental conditions, the net magnetic susceptibility of the ferritin-labeled lymphocytes in aqueous solution was 2.92×10^{-6}, and the ferritin load was 1.75×10^{7} molecules/cell. The net magnetic susceptibility of the ferritin-labeled lymphocytes was comparable to that of the deoxygenated erythrocytes, 5.17×10^{-6}.[7] It is interesting to note that for a reported lower ferritin load of 2.8×10^{4} ferritin molecules/cell, the paramagnetic susceptibility of ferritin was not sufficient to offset the diamagnetic susceptibility of the cell (assumed to be equal to that of the water, $\chi_{aq} = -9.05 \times 10^{-6}$), with a resulting predicted net magnetic susceptibility of the ferritin-loaded cell equal to -8.2×10^{-6} (diamagnetic).[37] The measured number of ferritin molecules per cell used in this study for magnetic separation provides the information needed for further applications of ferritin as a magnetic label and, in particular, in considering ferritin as an immunomagnetic label.

ACKNOWLEDGMENT

The authors thank Mr. Vernon C. Westcott and Drs. William W. Seifert and Robert S. Wenstrup for critical review of the magnetic field mapping, which resulted in the substantial revisions of the manuscript, and Mr. Lee R. Moore for proofreading the manuscript. This study was supported by NCI R01CA62349 and Whitaker Foundation grants.

GLOSSARY

a	interpolar gap half-width, eqs 7 and 8
b	intercept of the regression ϵ on ζ, eq 17
B	magnetic field intensity, eq 8
c	particle (cell) concentration
F	force
h	channel height
H	magnetic field strength
m	slope of the regression line ϵ on ζ, eq 17
n	sample size
r	radial coordinate, or correlation coefficient
N	number of ferritin molecules per lymphocyte, eq 5
P	complex potential, eq 6
Q	volumetric flow rate
R	hydraulic radius of the particle, eq 5
v	flow velocity
V	particle (cell) volume
w	channel width, or complex number on the w-plane, eqs 6 and 7
x,y	Cartesian coordinates
z	complex number on the z-plane, eqs 6 and 7

Greek Characters

ϵ	fractional cell recovery, eq 11
Θ	potential function in the complex potential P, eq 6
λ	relative distance from the deposition plate at entry, upstream and far away from the interpolar gap, eq 15 and Figure 3
λ_0	value of λ for the most distant trajectory ending at the deposition wall
$\Delta\chi$	effective magnetic susceptibility, averaged over particle volume, equal to a difference between the magnetic susceptibility of the particle and that of the medium (aqueous solution)
μ	magnetic moment
μ_0	magnetic permeability of vacuum, $4\pi \times 10^{-7}$ T/m·A
ϱ	specific density
η	viscosity of water
ζ	dimensionless number grouping the material and geometric constants of the magnetic deposition system
ζ_Q	proportionality constant between ζ and $1/Q$
ϕ	angular coordinate
Φ	field function in the complex potential P, eq 6

Subscript, Superscript, and Special Characters

aq	aqueous
av	average
D	viscous drag, or relating to the Dynabead
E	experimental
fer	ferritin
i	summation index
in, out	pertaining to quantities far away from the magnetic field
m	magnetic
0	saturation or initial value
1	relating to the proximal (deposition) wall of the deposition channel relative to the magnet surface
2	relating to the distal wall of the deposition channel relative to the magnet surface
′	dimensionless coordinate
$\langle\rangle$	average over spatial coordinates
boldface	vector quantity

Received for review March 13, 1995. Accepted July 26, 1995.[⊗]

AC950248K

(41) Meldrum, F. C.; Heywood, B. R.; Mann, S. *Science* **1992**, *257*, 522–523.

[⊗] Abstract published in *Advance ACS Abstracts,* September 1, 1995.